CHARACTERIZATION OF ETCHING PROCESS AND ETCH RATE OF ALUMINUM THIN FILM

BY

"RYAN" SUNGHO KANG

THESIS

Submitted in partial fulfillment of the requirements
for the degree of Bachelor of Science in Electrical Engineering
in the College of Engineering of the
University of Illinois at Urbana-Champaign, 2014

Urbana, Illinois

Adviser:

Songbin Gong

ABSTRACT

This thesis reports on characterization of etching process of aluminum thin film. It offers sequential steps of optimized etching process as well as the etch rate of aluminum thin film—one of the ubiquitous metals in MEMS and IC industries—for on-going RF MEMS research. To gain high device performance, an efficient and accurate fabrication process is critical. Despite a number of previous studies on etch rate characterization, unique tuning methods and fabrication recipes are required for different instruments and laboratories. In this report, the etching characterization is performed using PlasmaLab Master/Slave Reactive Ion Etching (RIE) System with flows of boron trichloride (BCl_3) and chlorine gas (Cl_2). Drawbacks of the tools and chemicals as well as corresponding adjustments are also discussed. Along with aluminum etch rate, etch rate of photoresist under the same parameters can also be evaluated in the same manner. The results of both etch rates are covered in this paper.

Subject Keywords: micro-electro-mechanical systems (MEMS); RF MEMS; micro-fabrication; etching; lithography; physical vapor deposition (PVD)

To my dad, for letting me study what I love.

ACKNOWLEDGMENTS

I would like to attribute this achievement and invaluable experience to my advisor, Prof. Gong, and his constant support and encouragement. Without Prof. Gong, I would not have been able to make a step into Micro and Nanotechnology Laboratory for this study and laboratory experience. Thanks to Prof. Gong and this research, I was able to discover my interests in MEMS, which I intend to continue studying.

I would also like to give special thanks to MNTL graduate students and staff engineers, especially Dr. Glennys Mensing and Dr. Yaguang Lian, who were always willing to help me with the tools whenever needed. Finally, I would like to express my gratitude to Electrical and Computer Engineering Department at University of Illinois for promoting undergraduate research by generously providing ECE Alumni Fund.

TABLE OF CONTENTS

LIST OF TABLES

LIST OF FIGURES

CHAPTER 1

INTRODUCTION

Micro-electro-mechanical systems (MEMS) constitute a young and growing research field. Microfabrication is an important part of such MEMS research due to its intrinsic properties. MEMS heavily depends on its mechanical and physical characteristics since many MEMS components, unlike integrated circuits (ICs), involve small-scale physical movements to be carefully sensed or actuated. Therefore, precise characterization of each microfabrication process is critical to device performance as well as accurate and effective research.

1.1 Aluminum

Metals are important building blocks in the MEMS and IC industries. Proper metals or metal alloys need to be employed to achieve various functionalities such as electrical and thermal conductors, sacrificial and structural materials, or optical reflectors [1]. Aluminum, the metal to be etched and examined in this paper, is also widely used in ICs as well as MEMS. Aluminum, along with aluminum nitride to be studied soon, in MEMS devices frequently serves as the electrode material in electrostatic sensor and actuator devices. Therefore, failure to find precise deposition or etch rates may result in poor device performance due to defects.

1.2 Microfabrication

Although etching process parameters for aluminum have been presented and discussed in many studies, they cannot simply be transferred directly across different

equipment or fabrication facilities [1]. Therefore, careful tuning of process parameters for different tools is very important in device fabrication. This paper reports on characterization of aluminum thin film etch using PlasmaLab Master Reactive Ion Etch (RIE) System in the cleanroom laboratory at the University of Illinois Micro and Nanotechnology Laboratory (MNTL). Based on the theories and previously done studies, an appropriate step-by-step fabrication recipe is suggested in this paper. Other tools and chemicals used in the process include Cooke Dual-Gun Sputter System, EVG Mask Aligner, AZ 1505 photoresist and AZ 400K developer. It is also important to note that various tools and chemicals have different mechanical and intrinsic limits and properties; furthermore they often affect recipe parameters such as development time, chamber pressure, or etching duration.

The overall process employs standard microfabrication, which consists of a properly ordered sequence of degreasing, metal deposition, photolithography, etching, and measurements and evaluation. First, aluminum thin film is deposited after the samples are properly cleaned and dried. Though metal deposition rate needs to be carefully examined to fabricate more sophisticated devices, this thesis approximates the deposition rate and deposits aluminum just thick enough to avoid over-etching. After the parts to be etched are defined in the photolithography step, reactive ion etching is performed. To effectively etch aluminum thin film, gas flows of boron trichloride (BCl_3) and chlorine (Cl_2) are employed. Etched aluminum and photoresist profile is realized using Tencor Alpha-Step IQ Profilometer and appropriate adjustments on etching recipe are made after each experiment step. Overall etch process is shown in Figure 1.1

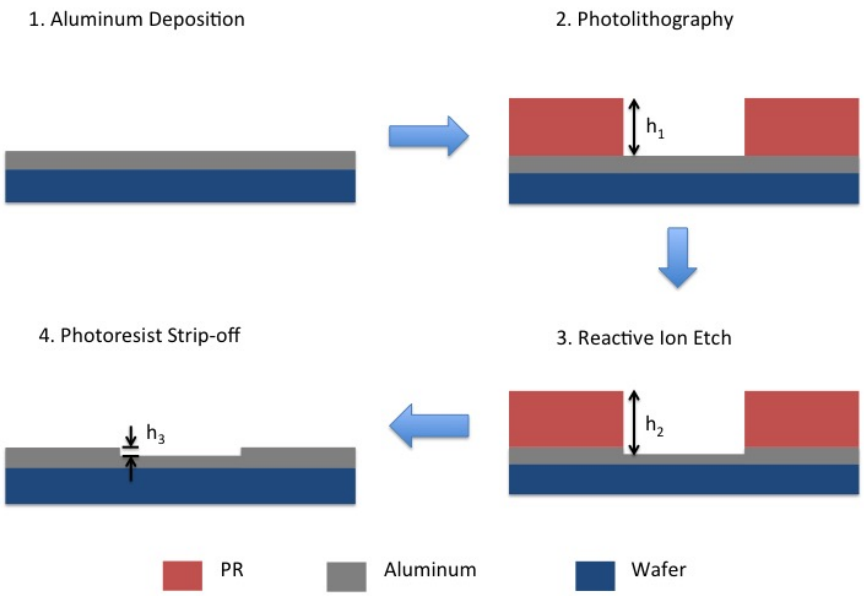

Figure 1.1: Flow chart of aluminum thin film etching process

CHAPTER 2

LITERATURE REVIEW

RF MEMS devices entered commercialization almost a decade ago, offering spectacular performance at microwave frequencies. Generally, RF MEMS offer lower power consumption and losses, along with higher linearity and quality factors than conventional communication components. Some of the successful RF components include: bulk acoustic wave devices, RF MEMS switches, and tunable capacitors [2]. Such devices allow for reconfigurability while miniaturizing the size and lowering power consumption. However, there also have been limiting factors for some of the RF MEMS devices.

RF MEMS switches, for example, in spite of the superior advantages they offer, have been hampered from quick deployment by two major limiting factors: reliability and packaging. Both capacitive switches and metal-contact switches are limited by dielectric charging and interface between the contact metals, respectively, giving 0.1–40 billion cycles; whereas many systems require 20–200 billion cycles [3]. Packaging has also been a major hurdle for RF MEMS switches, for the packaging methods for standard MEMS devices (gyroscopes, accelerometers, pressure sensors, etc) require a temperature of 300–400 °C; but this range of temperature may bow the membrane or cantilever, making the switch unusable [4]. Figure 2.1 [4] shows the packaging and interconnect schemes for the current MEMS switches.

There have been many studies on RF MEMS fabrication to improve the obstacles mentioned above. Aluminum, for example, is a commonly used metal in MEMS as well as ICs due to its high conductivity and low cost. Pure aluminum, however, exhibits low Young's modulus and poor surface morphology, which hin-

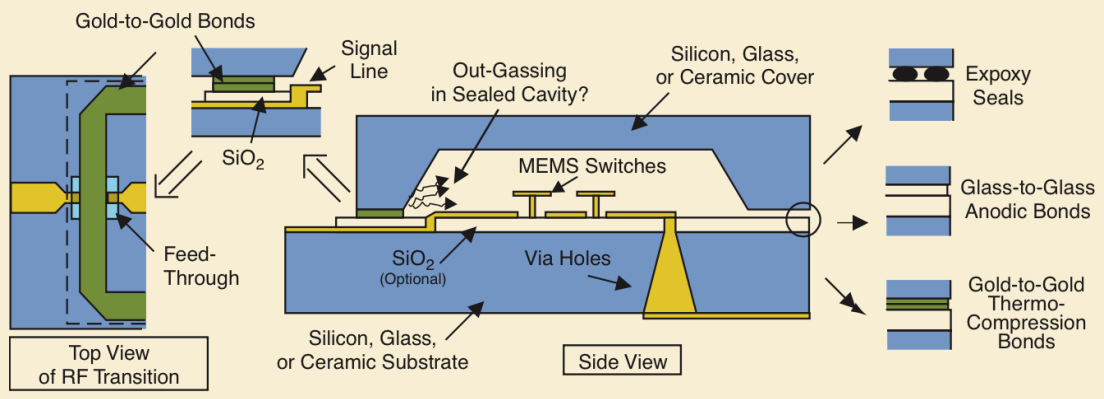

Figure 2.1: Packaging and interconnect schemes for current MEMS switches

der further utilization of aluminum as a piezoelectric material for RF MEMS. Recent studies by Kang *et al.* show effects of ion implantation on optical properties and hardness of aluminum thin film. The implantation of He or N_2 reduced global surface roughness at a moderate dose ($\sim 10^{16}$ ions/cm^2). With an appropriate implantation condition, aluminum also experienced increase in Young's modulus with N_2 ion implanted. Figures 2.2 and 2.3 show the results after N_2 implantation [5].

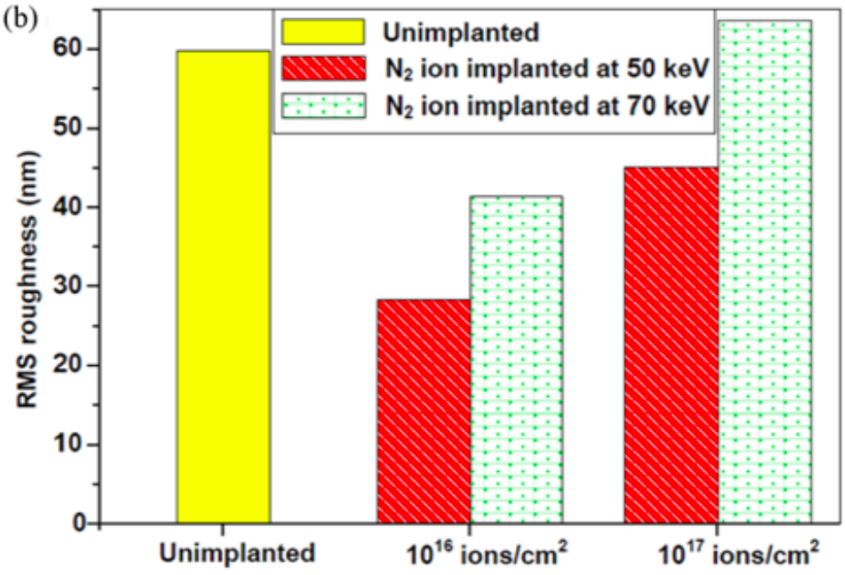

Figure 2.2: Global surface roughness of Al thin films after implantation of N_2 ions

The superior properties of aluminum nitride (AlN) have drawn significant at-

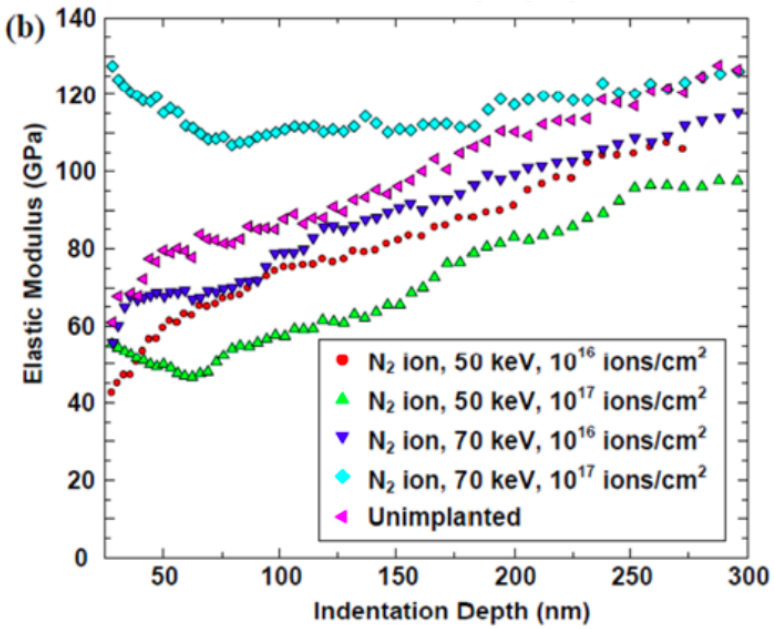

Figure 2.3: Young's moduli of Al thin films after implantation of N_2 ions

tention to RF applications, replacing contemporary piezoelectric materials such as lead zirconate titante (PZT) or zinc oxide (ZnO). Despite easy deposition techniques, the use of PZT and ZnO had been limited in RF applications due to their low quality factors and contamination risks in CMOS process. RF MEMS devices such as thin-film bulk acoustic resonators and reconfigurable oscillators (Figure 2.4 [6]) became commercially successful due to the unique properties of AlN [6]. Figure 2.5 [7] shows another ongoing RF resonator project at Northeastern Sensors & Nano Systems Laboratory. In this resonator, the use of aluminum nitride for the resonator allows for a high quality factor and compatibility with normal semiconductor process, whereas graphene (G) gives high electrical conductivity and low loss on an ultra-thin scale [7].

Chandra and Singh [8] have further presented characterization of aluminum nitride by RF magnetron sputtering for RF MEMS applications. Unlike PZT, AlN does not require poling, but rather its piezoelectric properties solely depend on crystal orientation. Integration of such MEMS devices with complementary metaloxide semiconductor (CMOS) has been a problem, though, due to high

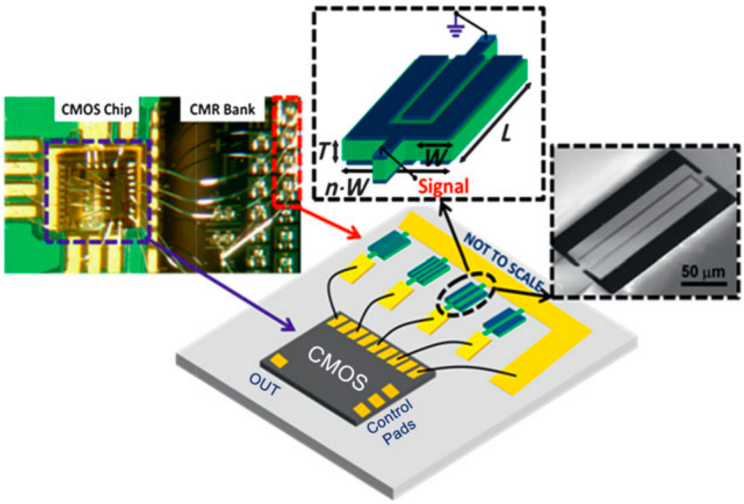

Figure 2.4: Reconfigurable CMOS oscillator based on AlN MEMS resonators

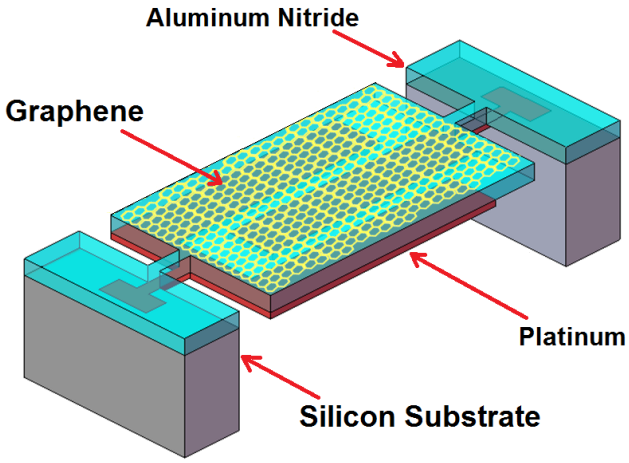

Figure 2.5: G–AlN hybrid nanoelectromechanical resonator

operating temperature during deposition of such piezoelectric materials. Chandra and Singh demonstrated preparation of ZnO and AlN without external substrate heating, which allows for post-CMOS process of MEMS.

CHAPTER 3

SIMPLE DEGREASE

Degreasing is a critical part in the fabrication process since it minimizes errors due to possible particle adhesion. Simple degrease is a widely used degreasing process in fast-paced research laboratories. Despite its faster procedure, it is very effective and efficient to minimize errors in characterization. Before each experiment, the following simple degrease sequence is performed on the samples.

1. Acetone : acetone removes organic residue from the wafer.
2. Isopropyl alcohol (IPA) : IPA dissolves acetone residue and other residues that are not soluble in acetone.
3. Deionized water : water dissolves IPA residue and other residues that are not soluble either in acetone and IPA.
4. IPA : this step is different from step 2 in that IPA here is used to ensure a faster dry using nitrogen in the next step.
5. Nitrogen gun : nitrogen gas dries wafer and prepare for the next step in fabrication.

CHAPTER 4

ALUMINUM DEPOSITION

4.1 Physical Vapor Deposition (PVD) and Sputter Deposition

Unlike chemical vapor deposition (CVD), physical vapor deposition involves the transfer of material and the formation of coatings by physical means alone [9]. Despite some of the inferior characteristics to CVD, PVD is still widely used in many research areas, especially for deposition of metals due to lower process risk and cheaper cost. PVD can be subdivided into evaporation and sputtering methods. While the evaporation method relies on the fact that source materials start to boil and evaporate at high temperature, the sputtering method makes use of ionized gas and its acceleration towards a target (source material) in plasma [10]. Once the chamber is set up so that high-energy ions—such as argon in this study—strike the target, the atoms from the target will be sputtered and deposited onto the wafers. In many sputtering systems, therefore, spacing between the cathode and anode is carefully controlled in order to optimize the amount of ejected atoms that would get deposited [9].

Along with the advantages of reliability and ability to cover topography compared to evaporation method, its operation at much lower temperature draws more attention for MEMS fabrication. Since many MEMS devices are integrated into conventional integrated circuits, high-temperature deposition methods are generally avoided. Low-pressure chemical vapor deposition (LPCVP) or evaporation deposition, for example, might result in permanent damage to IC due to its high operation temperature.

Table 4.1: Recipe used for Cooke Sputter

Pressure	5×10^{-6} Torr
RF Power (forward/reflected)	200/0 Watts
Time	8 minutes
Ar Gas Flow Rate	8 sccm
Expected Aluminum Thickness	$\sim$ 200 nm

4.2 Recipe for Cooke Dual-Gun Sputter System

In this experiment, a Cooke Dual-Gun Sputter System was used throughout the process to deposit aluminum thin film on the samples. Cooke Dual-Gun Sputter System is a physical vapor deposition tool that makes use of sputtering effect in vacuum chamber. Figure 4.1 [11] is the image of the tool at MNTL.

In order to get a constant surface roughness and minimize discrepancies throughout the samples, the same recipe specified in Table 4.1 was used to deposit aluminum on all samples. Since only an approximate value of thickness of aluminum was needed to test the etching effect, an accurate aluminum deposition rate was not found; instead, a rough estimate of the deposition rate ($\sim$25nm/min) was used.

Figure 4.1: Cooke Dual-Gun Sputter System

CHAPTER 5

PHOTOLITHOGRAPHY

The fundamental function of photolithography is to transfer a pattern of a mask into the wafer itself [12]. Since we only need unwanted area to be etched, precise patterning and lithography steps are essential. Photolithography can be subdivided into baking, spin-on photoresist, exposure, and development. Each process is explained in detail below.

5.1 Pre-bake

Pre-bake, sometimes called hard-bake, of wafer samples ensures that there is no moisture on the sample wafers before photoresist is coated. Any moisture remaining on a sample hinders photoresist from adhering tightly to the wafer. To remove any moisture on the samples before photoresist is applied, pre-bake at a higher temperature than soft-bake was done for a short period of time.

5.2 Spin on Photoresist

For a better result and accurate device fabrication, firm and smooth adhesion of photoresist is required. One common way to achieve this is by the use of adhesion promoter. In this experiment, AP 8000 adhesion promoter was applied on all wafers and spun before photoresist was coated. AP 8000 adhesion promoter has an amino-based functional group, enhancing adhesion between silicon and photoresist [13]. Once adhesion promoter is evenly applied, AZ 1505 positive photoresist is spin-coated at 3000 rpm. It is critical to have no air bubbles when

applying photoresist on wafers, as air bubbles may leave an area with uneven photoresist coated surface during spinning. Another factor that affects surface roughness and thickness of photoresist is the speed at which samples are spin-coated. Slow spinning may result in a non-uniform coated photoresist as well as edge beads at the outer edges of the sample wafers. Edge beads, in turn, might result in errors on mask aligner by hindering a closer and uniform contact during exposure. Though edge beads may be removed with simple tools, it is still desired to spin at a certain speed to minimize their occurrence.

5.3 Soft-bake

Soft-baking is another step to achieve stable adhesion between sample wafers and photoresist before the samples get exposed. Unlike the pre-bake step, soft-bake is done at a lower temperature, as photoresist coated samples on the pre-bake plate of a higher temperature may result in permanent damage to wafers.

5.4 Exposure

The photoresist coated wafers are then exposed under high-energy radiation (such as an ultraviolet ray, electron beams, or X-ray) before development. The high-energy light changes the chemical and mechanical properties of the photoresist that is not blocked by patterns on the mask. The two types of photoresist, positive and negative, determine whether the exposed polymer chains would break down or enhance bonding by cross-linking after exposure [14]. AZ 1505 photoresist used in this study is a positive photoresist, which will undergo the former—breakdown of polymer under exposure.

The lithography tool used in this paper, EVG 620 Mask Aligner (Figure 5.1), exposes the samples with i-line (wavelength of 365 nm) spectral lines that are filtered from mercury light source [15]. Detailed recipe with this tool is shown in Table 5.1.

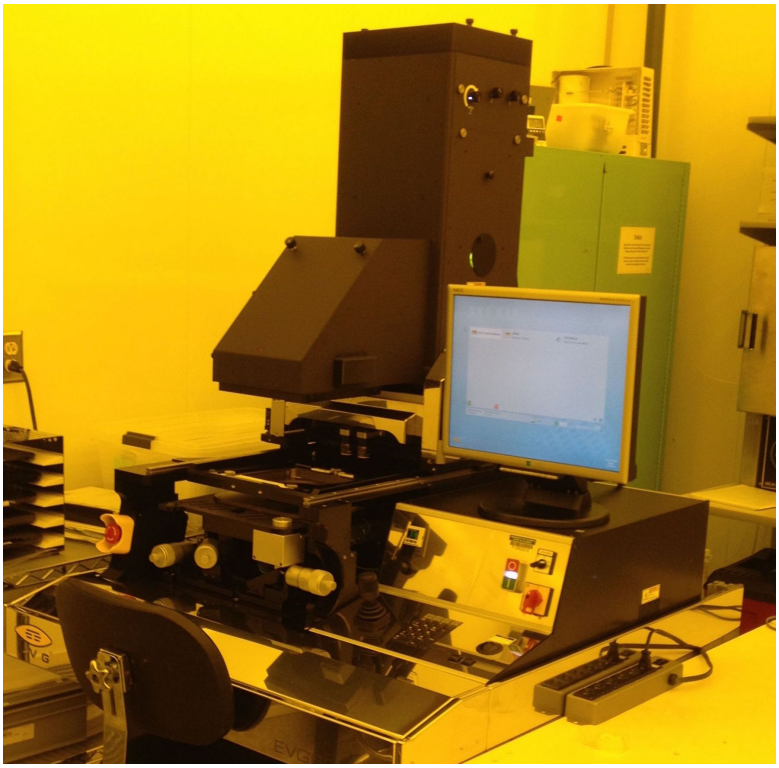

Figure 5.1: EVG 620 Mask Aligner

5.5 Development

After exposure, samples need to be exposed to define the patterns. Since AZ 1505 is a positive photoresist, the exposed area will be opened during development while unexposed area will remain attached to the sample wafers. Diluted AZ 400K developer was used in this experiment. Dilution rate was 4:1 (deionized water : AZ 400K developer). To optimize duration of development, multiple developments were tested all at different amounts of time. The optimized duration was found to be 20 seconds to avoid under- or over-development. When the target material to be etched is aluminum, however, one needs to give enough attention to avoid over-development, as AZ 400K etches aluminum at a finite rate around 0.74 nm/min (see Section 7.3).

5.6 Recipe

The recipe and parameters of photolithography from hardbake to development is summarized in Table 5.1.

Table 5.1: Parameters and recipe of photolithography

Hardbake	30 seconds, 150°C
AZ 1505	30 seconds, 3000 rpm, 250 rpm/s
EVG Mask Aligner	Top Side Align, 375 mJ/cm^2
Softbake	30 seconds, 110°C
Development (Diluted AZ400K)	20 seconds

CHAPTER 6

REACTIVE ION ETCHING

6.1 Reactive Ion Etching

Reactive ion etching is a dry etching process consisting of both physical and chemical methods. In RIE configurations, ions from the plasma are accelerated to high energy levels and high directionality towards the substrate [16]. Once the reactor chamber reaches low pressure by pumping, plasma is generated at radio frequency (RF). Typically, including the PlasmaLab RIE at MNTL, a frequency of 13.56 MHz is used as a standard [17].

6.2 Boron Chloride and Chlorine Gases

To effectively etch aluminum thin film, two gases BCl_3 and Cl_2 were used as etchants. Both play significant roles as etchants, forming volatile chemical compounds with aluminum and aluminum oxide. Chlorine gas in the reaction chamber is ionized into Cl^-s, resulting in volatile $AlCl_3$ from reaction with aluminum. During fabrication, formation of native aluminum is unavoidable and may hinder us from obtaining an accurate aluminum etch rate. This native aluminum oxide can be etched with the help of boron trichloride; BCl_3 reacts with Al_2O_3 and results in B_2O_3 as well as the same volatile gas $AlCl_3$ [18]. A summary of such chemical reactions is described in Equations (6.1) and (6.2).

Figure 6.1: PlasmaLab Master RIE System

Table 6.1: User input recipe for PlasmaLab Master RIE

BCl_3	33.8% (15 sccm)
Cl_2	9.4% (8 sccm)
Pressure	15 mTorr
RF Power	20% (60 W)

$$2Al + 3Cl_2 \rightarrow 2AlCl_3 \uparrow \tag{6.1}$$

$$2BCl_3 + Al_2O_3 \rightarrow B_2O_3 + 2AlCl_3 \uparrow \tag{6.2}$$

6.3 Recipe for PlasmaLab Master RIE System

PlasmaLab Master RIE System (Figure 6.1 [19]) showed some irregular discrepancies of values between user input parameters and the actual values at which the PlasmaLab Master RIE etched. The user input value (target recipe) was set to be the same for all three samples, with the exception of etching time. Table 6.1 is the target recipe for Plasmalab Master RIE System.

Etching time was set to be 90 seconds (1.5 minutes), 2 minutes, and 4 minutes for the samples A, B and C, respectively. Use of different etching times was to ensure that consistent and accurate data is obtained. Table 6.2 shows the actual parameter values of PlasmaLab Master RIE on each sample. Note that the biggest

Table 6.2: Actual recipe parameters for sample A, B, and C

	Sample A	Sample B	Sample C
BCl_3	15.63 sccm	15.67 sccm	15.63 sccm
Cl_2	7.45 sccm	7.23 sccm	7.32 sccm
Pressure	26 mTorr	26 mTorr	26 mTorr
RF Power	61.3 W	50 W	58.7W
Time	1.5 minutes	2 minutes	4 minutes

discrepancy was the chamber pressure. Although the target pressure was set to 15 mTorr, the actual chamber pressure turned out to be 26 mTorr; where the limit of PlasmaLab Master RIE is reached at around 25 mTorr.

6.4 Conversion Factors

PlasmaLab Master RIE accepts user input parameters in percentage, which in turn will be converted into sccm (standard cubic centimeters per minute) flow rate. The flow rate of gases traveling through each gas pipeline is controlled by MFC (Mass Flow Controller) and each MFC indicates relative flow rate of nitrogen gas when input pressure parameter is 100%. Etchant gases in this experiment went through the same type of MFC in which 100 sccm of nitrogen gas was ensured to flow when input pressure parameter is 100% (the conversion factor of nitrogen gas is 1.001 sccm/&; 100 sccm = 1.001 sccm%$\times$ 100 %). In the same manner, one can adjust the flow rates of other gases using the conversion factors. The calculations to obtain gas flow rates of BCl_3 and Cl_2 are shown in Equations (6.3) and (6.4), where the conversion factors of BCl_3 and Cl_2 are 0.444 and 0.851, respectively [20].

$$r_{BCl_3} = 0.444[\%/sccm] \times 33.8[\%] = 15[sccm] \quad (6.3)$$

$$r_{Cl_2} = 0.851[\%/sccm] \times 9.4[\%] = 8[sccm] \quad (6.4)$$

CHAPTER 7

RESULTS

7.1 Profilometer

A profilometer is an instrument that measures surface profiles and roughness with optical and/or contact methods. The Tencor IQ Profilometer used in this study is of the contact method, where a diamond stylus physically touches and moves along the sample to measure the surface profile. Although profilometers using the contact method may lead to slight surface damage or wear, their ease of use and high resolution have increased their popularity.

7.2 Results of Samples A, B, and C

To obtain etch rate, height differences were measured three times for each sample throughout the experiment. First, the height of the photoresist (h_1) coating was measured after development. The photoresist was found to be slightly thicker than suggested (0.58 μm at spin speed 3000 rpm) in the handbook [21]. Then, after reactive ion etching, etched photoresist and aluminum thicknesses (h_2) were measured together. The first two steps were performed to find etch rate of AZ 1505 photoresist under the same recipe used for aluminum etching. Once photoresist was stripped off after the same sequential steps as done in simple degreasing, the etched thickness of aluminum (h_3) was measured. Profilometer measurements are shown in Figure 7.1. With these measurements from profilometer, one can calculate aluminum etching rate as well as photoresist etch rate. Equations (7.1) and (7.2) were used to calculate the etch rates of aluminum and photoresist,

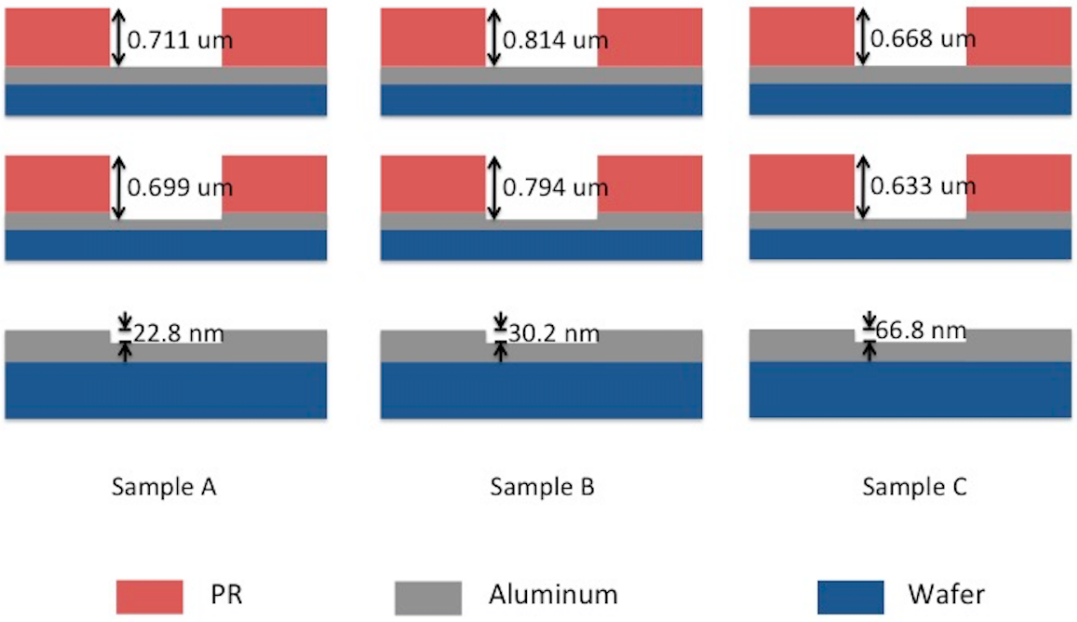

Figure 7.1: Height changes of the samples after each processing step

respectively.

$$r_{Al} = \frac{h_3}{t} \tag{7.1}$$

$$r_{PR} = \frac{h_1 - (h_2 - h_3)}{t} \tag{7.2}$$

As explained above, h_1 refers to the original height of photoresist after development. $h_2 - h_3$ is the height of photoresist after reactive ion etch; therefore the difference between h_1 and $h_2 - h_3$ is the height to which photoresist was etched due to the reactive ion etching under flows of BCl_3 and Cl_2. Along with Figure 7.1, Table 7.1 shows the measurements and calculations of samples A, B and C.

With the calculations in Table 7.1, the average etching rates can be calculated. Equations (7.3) and (7.4) show the calculations and the averaged etching rates of aluminum and PR, respectively. The summarized resulting etch rates of Al, AZ 1505 photoresist as well as the effect of AZ 400K are shown in Table 7.2.

Table 7.1: Profilometer measurement values and the etch rates calculated

	Sample A	Sample B	Sample C
h_1	0.711 μ m	0.814 μm	0.668 μm
h_2	0.699 μ m	0.794 μm	0.633 μm
h_3	22.8 nm	30.2 nm	66.8 nm
Al Etch Rate	15.2 nm/min	15.1 nm/min	16.7 nm/min
PR Etch Rate	23.2 nm/min	25.1 nm/min	25.45 nm/min

Table 7.2: Summarized results of etch rates and the effect of AZ400K

Aluminum Etch Rate	15.7 nm/min
AZ1505 Photoresist Etch Rate	24.6 nm/min
AZ400K (4:1 Diluted) Aluminum Etch Rate	0.74 nm/min

$$r_{Al,avg} = \frac{r_{Al,A} + r_{Al,B} + r_{Al,C}}{3} = 15.67[\text{nm/min}] \quad (7.3)$$

$$r_{PR,avg} = \frac{r_{PR,A} + r_{PR,B} + r_{PR,C}}{3} = 24.58[\text{nm/min}] \quad (7.4)$$

7.3 Aluminum Etch Rate Due to AZ 400K Developer

The effect of AZ 400K developer on aluminum is discussed more in depth in this section. AZ 400K developer used for development in this study has a non-negligible effect on aluminum, as it intrinsically has a finite aluminum etch rate [22]. The following experiment used 4:1 (DI water : AZ 400K) diluted AZ 400K developer, the same dilution rate as used to develop the samples A, B and C.

First, a dummy wafer with some aluminum etched is measured with a profilometer to obtain the height difference of aluminum thin film due to the etching effect. The difference in height is shown in Figure 7.2. After the height difference is measured, the sample is submerged in the diluted AZ 400K developer until a bare silicon starts to appear. Due to the etching effect of the developer, aluminum on the dummy sample will get etched away uniformly. Therefore, a bare wafer will start to appear first in the area with thinner aluminum, which gives the height of

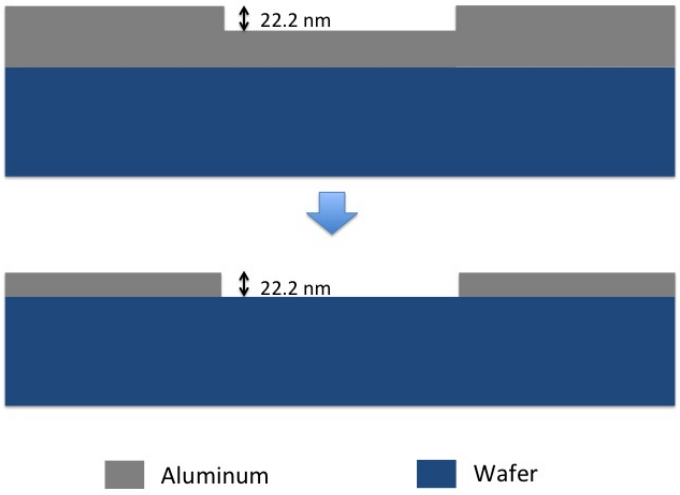

Figure 7.2: Profilometer measurement of the dummy sample

etched aluminum and its corresponding duration of development time. The result shows that 22.2 nm of aluminum was etched due to the AZ 400K developer in 30 seconds. Equation (7.5) shows the simple calculation used to obtain the etching effect of the developer.

$$r_{Al,AZ400K} = \frac{22.2[\text{nm}]}{30[\text{seconds}]} = 0.74[\text{nm/s}] \tag{7.5}$$

CHAPTER 8

CONCLUSION

In this paper, the etch rates of aluminum and photoresist (AZ 1505) were studied with the recipe described. The etching process includes metal deposition (physical vapor deposition), photolithography (exposure and development), and reactive ion etch. Each step was followed by a measurement using p/a rofilometer to obtain the changes in height of photoresist and aluminum. The recipes for metal deposition and photolithography were fixed for all samples, whereas the duration of etching in the reactive ion etch step was varied to obtain more precise data.

The results show a consistent etch rate throughout the samples. With the three samples, the average aluminum etch rate was calculated to be around 15.7 nm/min and the average photoresist etch rate 24.6 nm/min. The effect of AZ 400K developer was also found to be critical and therefore was discussed in depth. Due to its chemical properties, some metals—including aluminum—are prone to be etched by the developer at a finite rate including aluminum.

Obtaining accurate etch rate data as discussed in this paper is critical in many device fabrications including IC and MEMS. Aluminum, along with aluminum nitride, is a widely used material as conductor and piezoelectric material in both IC and MEMS. Further studies might include finding a more precise effect of reactive ion etcher that allows a lower chamber pressure and/or ICP (inductively coupled plasma). One can also perform the same experiment using different developer to minimize the non-negligible effect of metal etch rate of AZ 400K, which in turn will optimize more complex fabrication process.

REFERENCES

[1] R. Ghodssi, P. Lin et al., *MEMS Materials and Processes Handbook*, ser. MEMS Reference Shel. New York, NY: Springer, 2011.

[2] J. Bouchaud and H. Wicht, "RF MEMS: Status of the industry and roadmaps," *IEEE Radio Frequency Integrated Circuits Symposium*, pp. 379–384, 2005.

[3] G. Rebeiz, "RF MEMS switches: status of the technology," in *Solid-State Sensors, Actuators and Microsystems, 12th International Conference on, 2003*, vol. 2, June 2003, pp. 1726–1729.

[4] G. Rebeiz and J. B. Muldavin, "RF MEMS switches and switch circuits," *Microwave Magazine, IEEE*, vol. 2, no. 4, pp. 59–71, Dec 2001.

[5] T. J. Kang et al., "Butt-jointed DBR laser with 15 nm tunability grown in three MOVPE steps," *International Journal of Precision Engineering And Manufacturing*, vol. 15, no. 5, pp. 889–894, 2014.

[6] G. Piazza et al., "Piezoelectric aluminum nitride thin films for microelectromechanical systems," *Materials Research Society*, vol. 37, pp. 1051–1061, 2012.

[7] "Graphene-Aluminum Nitride (G-AlN) Hybrid Nanoelectromechanical Resonator and its Applications," 2014. [Online]. Available: http://www.northeastern.edu/nemslab/research/

[8] S. Chandra and A. V. Singh, "Preparation and Characterization of Piezoelectric Films of ZnO and AlN by RF Sputtering for RF MEMS applications," *Key Engineering Materials*, vol. 500, pp. 84–89, 2012.

[9] S. A. Campbell, *Fabrication Engineering at the Micro- and Nanoscale*, ser. Oxford series in Electrical and Computer Engineering.

[10] "Mems thin film deposition processes," 2014. [Online]. Available: https://www.mems-exchange.org/MEMS/processes/deposition.html

[11] "Cooke dual-gun sputter system," 2014. [Online]. Available: http://mntl.illinois.edu/equipment/cooke_sputter.htm

[12] D. R. Hines, N. P. Siwak, L. A. Mosher, and R. Ghodssi, *MEMS Lithography and Micromachining Techniques*, ser. MEMS Reference Shel. New York, NY: Springer, 2011.

[13] J. M. Snodgrass and R. H. Dauskardt, "The effect of fatigue on the adhesion and subcritical debonding of benzocyclobutene/silicon dioxide interfaces," *International Journal of Precision Engineering and Manufacturing*, vol. 612, pp. D1.3.1–D1.3.6, 2000.

[14] C. Liu, *Foundations of MEMS*. Upper Saddle River, NJ: Pearson, 2005.

[15] "Evg 620 mask aligners," 2014. [Online]. Available: http://mntl.illinois.edu/equipment/EVG-Aligner.htm

[16] T. M. Adams and R. A. Layton, *Introductory MEMS*. New York, NY: Springer, 2010.

[17] S. Gao, "Dry etching and reactive ion etching," Feb. 2013. [Online]. Available: http://www.cse.wustl.edu/ vgruev/cse/506/slides/w4_dry_etching.pdf

[18] H. Shih, *A Systematic Study and Characterization of Advanced Corrosion Resistance Materials and Their Applications for Plasma Etching Processes in Semiconductor Silicon Wafer Fabrication*. Rijeka, Croatia: InTech, 2012.

[19] "Plasmalab master / slave dual-chamber reactive ion etcher," 2014. [Online]. Available: http://mntl.illinois.edu/equipment/pl_rie.htm

[20] "Gas correction factors for thermal-based mass flow controllers," 2014. [Online]. Available: http://www.mksinst.com/docs/ur/MFCGasCorrection.aspx

[21] "Az 1500 series data sheet," 2013. [Online]. Available: http://www.first.ethz.ch/infrastructure/Chemicals/Photolithography/Data_AZ1500.pdf

[22] "Az developer, 400k, and 421k inorganic developers," 2002. [Online]. Available: https://www.clean.cise.columbia.edu/process/inorgdev.pdf